ACS Catalysis

Research Article

pubs.acs.org/acscatalysis

Nanoparticulate TiO_2–Al_2O_3 Photocatalytic Media: Effect of Particle Size and Polymorphism on Photocatalytic Activity

M. Bouslama,[†,‡] M. C. Amamra,[†] Z. Jia,[†] M. Ben Amar,[†] K. Chhor,[†] O. Brinza,[†] M. Abderrabba,[‡] J.-L. Vignes,[†] and A. Kanaev*[,†]

[†]Laboratoire des Sciences des Procédés et des Matériaux C.N.R.S., Université Paris 13, Sorbonne Paris Cité, 93430 Villetaneuse, France

[‡]Laboratoire de Physico-chimie Moléculaire, Institut Préparatoire aux Etudes Scientifiques et Techniques, Université de Carthage, Tunisie

ABSTRACT: Impregnation of size-selected titanium-oxo-alkoxy nanoparticles into monolithic ultraporous alumina (UPA) permits nanoparticulate photocatalytic media with an extended activity into the high-temperature range up to 1000 °C, which is explained by anatase TiO_2 phase stability due to the inhibited nanoparticles aggregation. In this Article we report on the effect of the nanoparticle polymorphism and size on the photocatalytic ethylene gas decomposition. Use of UPA supports of γ, θ, and α polymorphs, covered with silica or not, and thermal treatment at different temperatures allow modification of the nanoparticles size and crystalline composition. In all cases, the interaction between titania and UPA support is found to affect the polymorph stability. In particular, a separating layer of silica increases the temperature of the anatase-rutile transformation. The main conclusion is that anatase nanoparticles exhibit the higher activity compared to rutile and composite anatase/rutile nanoparticles. The rutile activity strongly decreases with size $2R \geq 5$ nm, while that of anatase nanoparticles does not appreciably change for sizes 5 nm $\leq 2R \leq$ 10 nm. The material activity strongly decreases when rutile phase is nucleated onto the anatase one.

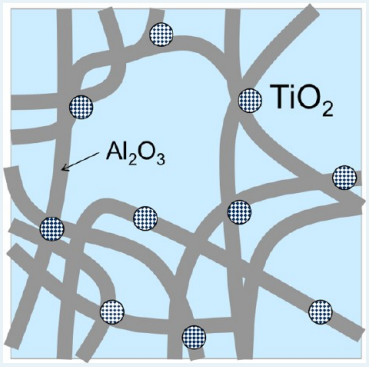

KEYWORDS: *TiO_2 nanoparticles, anatase and rutile polymorphs, ultraporous alumina, photocatalytic activity, size effect*

1. INTRODUCTION

Titanium dioxide (TiO_2) crystalline solids are of permanent interest in photocatalysis.[1−3] An issue of their optimal structural composition and particle size has been raised after successful synthesis of Degussa P25 mixed-phase industrial product, reputed as most active and therefore widely used in the related research as the reference sample. In fact, this powder is composed of agglomerated primary crystalline TiO_2 particles of 15−30 nm size with major anatase (∼70%) and minor rutile (30%) content in presence of a small amount of the amorphous phase.[4,5] The amorphous phase is generally accepted as inactive.[6] Attempts to explain the photocatalytic activity of Degussa P25 and further improve the activity of mixed-phase titania are under way.[7−12] An improvement of the photocatalytic activity was attributed to dynamics of the electron−hole recombination process,[13] specific area of the materials, and different reactivities of crystalline facets in radicals' generation.[14] Moreover, small size and narrow polydispersity of TiO_2 particles have important consequences on the photocatalytic efficiency. Generally, small nanoparticles of $2R \leq 10$ nm are privileged;[15,16] however, larger nanoparticles can exhibit relatively better activity because of an improved crystalline quality.[17] At the same time, most recent comparison between pure and mixed-phase crystalline titania nanoparticles has shown a clear advantage of pure anatase polymorph and dominant contribution of crystalline quality on the photo-induced charge carriers lifetime and consequently, photocatalytic efficiency.[8] Changes of the electronic band structure with TiO_2 particle size can be disregarded.[18,19]

An analysis of different factors that affect the material activity is difficult because of their coupling. In particular, the particle size can also strongly affect its crystalline quality and phase. As it has been shown, the size can invert phase stability and anatase becomes stable compared to rutile for particle smaller than ∼14 nm.[20,21] At the same time, a comparison of anatase titania particles of size between 7 and 300 nm has indicated a decrease with the size of their thermal stability toward phase transformation into the stable rutile.[22]

The tendency of the oxide nanoparticles toward agglomeration is very strong, and most of the existing methods for the nanoparticles preparation results in powder-like products with micrometer-sized aggregates of the primary nanoparticles. Their individual responses are often found strongly inhibited in these conditions. In particular, crystalline facets of nanoparticles exhibit different photocatalytic and aggregation activities and new phase nucleates at the grains boundaries.[23] Moreover, influence of the support composition and morphology is of importance since nanoparticle immobilization

Received: January 16, 2012
Revised: June 29, 2012
Published: July 23, 2012

 © 2012 American Chemical Society

Table 1. Prepared Photocatalysts Samples and Specific BET Areas before (σ_a) and after Titania Impregnation (σ_c)[a]

sample	temperature of treatment (°C)	treatment by silica	UPA polymorph	σ_a (m^2/g)	TiO_2 loading wt %	σ_c (m^2/g)
A	1150	+	γ	170	24	170
B	1150	−	θ	110	23	115
C	1300	+	θ	110	26	115
D	1300	−	α	10	5.2	10

[a]Values for samples B, C, and D were previously reported.[25].

often results in undesirable losses of the photocatalytic efficiency.[24] Elaboration of size-selected nanoparticles and their immobilization by preserving against aggregation is a challenging task in the field of photocatalysis.

Recently, we have reported on a method of preparation and immobilization of size-selective TiO_2 nanoparticles, free of aggregation, into ultraporous alumina (UPA) monoliths.[25] In this work we made a comparison of photocatalytic activities of titania nanoparticles of different mass loadings into ultraporous alumina and thermally treated at 400−500 °C and then we have shown a stability of anatase nanoparticles in silica-treated θ-alumina matrix at higher temperatures. In the present article we report on a systematic study of these promising TiO_2−UPA nanomaterials: in particular, we examine the influence of different UPA matrixes of γ, θ, and α crystalline phases on the size, polymorphysm, and photocatalyst activity of immobilized TiO_2 nanoparticles thermally treated in the range between 400 and 1300 °C.

2. EXPERIMENT

2.1. Photocatalyst Preparation. High-purity ultraporous alumina samples were obtained at room temperature, in humid atmosphere (relative humidity 70−80%), by oxidation of aluminum plates through a liquid mercury−silver layer.[26,27] To increase the mechanical rigidity, chemical and thermal treatment of the raw materials was used. The chemical treatment has been achieved by homogeneous impregnation of gaseous trimethylethoxysilane (TMES: $(CH_3)_3$-Si-C_2H_5O). As a result, the silicon alkoxide is hydrolyzed at the hydrated alumina surface resulting in the structure coverage by ∼6 wt % silica. The thermal treatment leads to the UPA monoliths of known γ, θ, and α polymorphs. In particular, θ and α polymorphs appear at thermal treatment of the raw material at 1100 and 1200 °C, respectively; however, the silica-treated UPA extends stability of γ and θ polymorphs until 1200 and 1400 °C, respectively. Four UPA samples were prepared for the following impregnation of titania nanoparticles: γ (treated by silica and thermally at 1150 °C), θ (treated thermally at 1150 °C), θ (treated by silica and thermally at 1300 °C), and α (treated thermally at 1300 °C) polymorphs.

Size-selected 5.2-nm titanium-oxo-alkoxy nanoparticles were prepared in a sol−gel reactor described in refs 28−30. The reactor operates in the turbulent injected mode of reacting fluids with Reynolds number $Re = 4500$ ($Re = 4Q\rho/\pi\eta d$, where Q, ρ, and η are the fluid flow rate, density, and dynamic viscosity). The reactor temperature is fixed at 20.0 °C and hydrolysis ratio $H = C_W/C_{Ti} = 2.2$, where $C_{Ti} = 0.146$ M and C_W are titanium tetra-isopropoxide (TTIP) and water concentrations, respectively. This regime corresponds to small Damköhler numbers $Da = r_{Ch}/r_{Ph} \leq 1$, which guarantees the rate of the physical process "mixing" r_{Ph} being higher than that of hydrolysis−condensation reactions r_{Ch} leading to nucleation. The particle size was monitored in situ by photon-correlated spectroscopy, using a homemade monomode optical fiber probe and 32 bits 288 channels digital correlator Photocor-FC with software Dynals. The observation volume defined by a mutual positioning of two monomode optical fibers is small enough (∼10^{-6} cm^3) to prevent multiple scattering events even at high particle concentrations. TTIP and 2-propanol of 98% purity (Acros Organics) and distillated water were used in experiments.

The photocatalysts were prepared by three repetitive cycles *colloid impregnation-drying* of four selected UPA matrixes, which permit the adjustment of the desirable titania mass, followed by the thermal treatment of the catalyst at different temperatures (during 4 h) to obtain titania with desirable polymorphs and crystalline size. This procedure has been described in ref 25. Strong covalent bonds formed between surface hydroxylated sites of the titanium-oxo-alkoxy nanoparticle and UPA matrix ensure mechanical stability of the catalyst. In agreement with our earlier results,[25,31] specific area of nanoporous catalysts is not affected by the nanoparticles' impregnation using this method.

The loaded catalysts, cut in pellets of ∼1−2 mm size, were thermally treated in the temperature range between 400 and 1200 °C for 4 h, which does not alter the alumina matrix characteristics but triggered TiO_2 growth and phase transformation from amorphous to anatase and to rutile polymorphs. The temperature increase during this treatment was 300 °C/h before to attain the plateau, and the temperature decrease down to the room temperature after the treatment was free.

Four photocatalyst samples labeled A, B, C, and D were prepared as summarized in Table 1. The specific area was measured by the Brunauer−Emmett−Teller (BET) method (Coulter SA3100), and the deposited TiO_2 mass was measured by the ammonium sulfate NH_4SO_4-sulfuric acid H_2SO_4 digestion method.[32,25] Except for the TiO_2−UPA(α) sample, which has much higher mass density and lower specific area, other TiO_2−UPA(γ-silica), TiO_2−UPA(θ), and TiO_2−UPA(θ-silica) samples allow much higher titania mass loadings close to ∼25 wt % compared to 5.2 wt % for the first one.

2.3. Photocatalyst Characterization. The nanoscale morphology of the prepared samples was characterized using JEOL2011 high resolution transmission electron microscopy (TEM) operated at 200 KeV with LaB_6 emission source of electrons. Element maps (Ti) of the samples were obtained using energy filtered TEM (EFTEM) with a Gatan Imaging Filter 2000 system connected to a transmission electron microscope. The energy and spatial resolutions of the system were 1 eV and 1 nm, respectively.

The samples were structurally characterized by the X-ray diffraction (XRD) method on an INEL XRG 3000 installation using Co−Kα (λ = 1.789 Å) radiation source.

UV−visible absorption spectra were measured by an optical fiber probe using D_2 lamp (Oriel). The fiber transmits the signal to a Cromex monochromator (grating 150 L/mm, f = 30 cm, slit 20 μm) coupled to a CCD detector (Princeton).

dx.doi.org/10.1021/cs300033y | ACS Catal. 2012, 2, 1884−1892

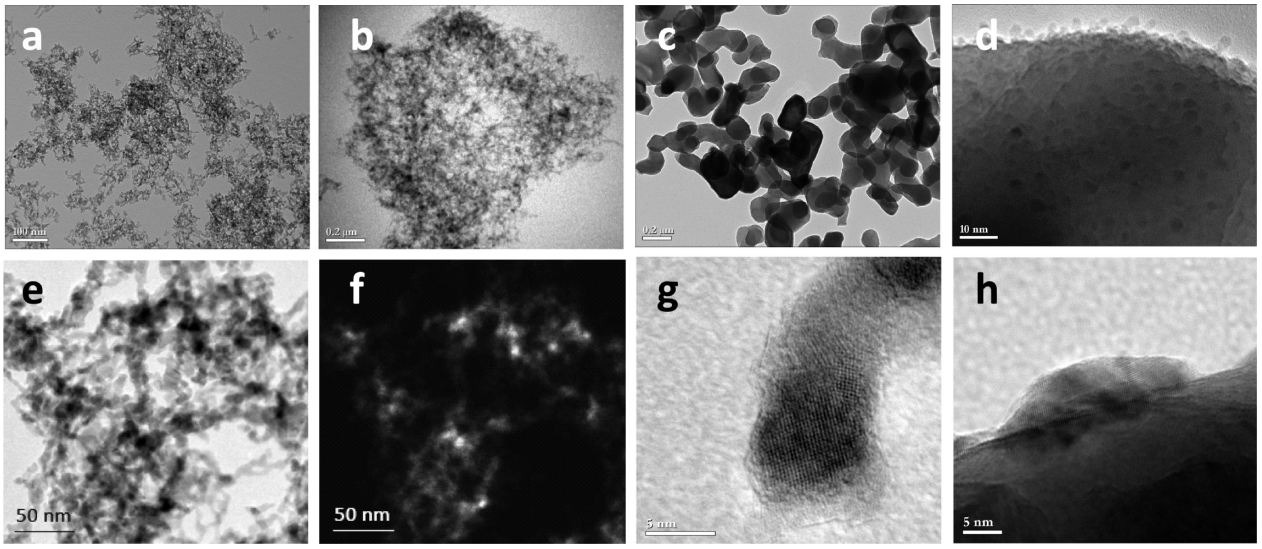

Figure 1. TEM images of nanocomposites TiO_2−UPA(γ)-SiO_2 (a), TiO_2−UPA(θ)-SiO_2 (b), and TiO_2−UPA(α) (c−d,h) and TiO_2−UPA(θ) (e−g). Ti elemental map of (e) is shown in EFTEM image (f). High-resolution TEM images of TiO_2 on UPA(θ) (g) and UPA(α) (h). Samples a−g and h are respectively treated at 600 and 800 °C after the nanoparticles' impregnation.

The photocatalytic activity of the prepared samples was tested in a continuous-flow fixed-bed reactor[33] on ethylene decomposition. A gas flow of pollutant (36 ppm) mixture with dry air (1 atm) and flow rate of 75 mL/min passes through a reactor tube of 6-mm diameter made of glass transparent in the UV-A spectral range. The photocatalyst samples labeled A, B, C, and D (see Table 1) with total deposited TiO_2 masses of 120, 105, 125, and 90 mg, respectively, were cut in pellets of 1−2 mm size and filled the reactor tube of 15 cm length. The tube is surrounded at a radial distance of 3 cm by six 8-W lamps emitting at 362 nm ($\Delta\lambda_{hwfm}$ = 22 nm). The reactor temperature 46 ± 2 °C was maintained during the experiments. Ethylene concentrations before (C_{in}) and after (C_{out}) the photocatalytic reactor were monitored by online gas chromatography (Varian CP 3800) equipped with a capillary column (HP-PLOT/Q) and a flame ionization detector FID. Two injection loops of 250 μL and heated at 80 °C allow measurements of pollutant concentration in continuous mode. Column temperature and carrier gas (N_2) flow rate are respectively 50 °C and 5 mL/min. The LI-820 gas analyzer was used for a continuous monitoring of the CO_2 concenration at the reactor output.

Since the ethylene conversion follows first-order kinetics in these experimental conditions,[16] the reactivity ($R = k\tau$, where k is the reaction rate constant and τ∼1.2 s is the pollutant residence time in the reactor bed) was calculated by the expression

$$R = \ln(C_{in}/C_{out}) \quad (1)$$

The specific reactivity was obtained by normalization of the reactivity on the total deposited TiO_2 mass:

$$r_S = \frac{\ln(C_{in}/C_{out})}{m_{TiO_2}} \quad (2)$$

As we pointed out in refs 16,25 this formula is equivalent to the expression generally used in photocatalytic studies: *rate* = $W(C_{in}-C_{out})$ (W stands for the volumetric gas flow) since *rate* ≡ kN (N is the total number of the pollutant molecules in the reactor volume during reactor run). Consequently, the proposed expression (2) permits direct analysis of the material activity since *rate* is a function of the variable N.

The experimental reproducibility $\Delta(C_{out}/C_{in})/(C_{out}/C_{in})$ = ±6% was checked with different fills of the reactor bed volume with the same type of photocatalyst samples. We have measured only the ethylene concentrations. However, the mineralization yield $(C_{CO2})_{out}/2((C_{C2H4})_{in} - (C_{C2H4})_{out})$ = 75−80% was typical of the present experiments. Our separate measurements have shown that CO and CO_2 constitute almost totally the reaction products of the ethylene decomposition (yield close to 100%). No reaction has been observed in dark conditions with UV lamps "off". Additionally, we have checked that the reactor performance is not strongly influenced by the photocatalyst pellets size. Indeed, the same photocatalytic and mineralization yields were observed when the pellets were milled down to a size of <500 μm.

3. RESULTS AND DISCUSSION

3.1. Structural Photocatalyst Modifications. The TEM images (Figure 1) show nanoscale morphologies of the prepared samples A, B, C, and D, which are quite different. The microstructure of the raw UPA material with specific area 300 m^2/g consists of tangled hydrated alumina fibers with a diameter of about 5 nm.[26] After crystallization of γ and θ polymorphs, the average grain size increases until about 8−10 nm and the specific area of samples A, B, and C becomes 170, 110, and 110 m^2/g, respectively, (Figure 1a−b,e). This is quite different from the morphology of sample D, which crystallized into an α-alumina polymorph (Figure 1c). It consists of grains of a size of ∼200 nm with the reduced specific area of 10 m^2/g. While the A, B, and C samples are very aerated with a large porosity and a low mass density of 0.15 g/cm^3, sample D is less porous with mass density of 0.6 g/cm^3, which explains its mechanical tightness. Samples A, B, and C are fragile but can be easily manipulated.

The impregnated 5-nm TiO_2 nanoparticles can be clearly seen on the large grains of α-alumina in Figure 1d. They cover the support with small mutual separation. The observation of TiO_2 nanoparticles in TEM images of samples A, B, and C is difficult because their nanoscale structural units have similar

dx.doi.org/10.1021/cs300033y | ACS Catal. 2012, 2, 1884−1892

size. However, the TiO_2 nanoparticles can be readily identified in the EFTEM images, one of which of sample B is shown in in Figure 1f (Ti map). The high-resolution TEM image of one nanoparticle (anatase, treated at 600 °C) in sample B is shown in Figure 1g. According to the presented images, the TiO_2 nanoparticles are well dispersed in the matrix without appreciable mutual contact. This last morphology is favorable to the nanoparticle's isolation and aggregation suppression at thermal treatment of the photocatalyst, which results in the crystalline phase's inversion recently reported by Bouslama et al.[25] One can also expect the usual polymorph's appearance at thermal treatment of sample D, similar to that observed in coatings and powders. In particular, the impregnated nanoparticles in sample D begin to aggregate when thermally treated at 800 °C (Figure 1h).

To confirm this statement about weak nanoparticle aggregation, we have measured XRD patterns of the prepared samples after different temperatures of the thermal treatment from 400 to 1200 °C. The rutile ratio of samples A, B, C, and D were calculated from the XRD intensity data by the equation $F_r = 1 - (1 + 1.265I_{r110}/I_{a101})^{-1}$.[35] The patterns of two of them, A and B, are shown in Figure 2 (a) and (b), respectively, in the range of the main anatase 101 and rutile 110 peaks.

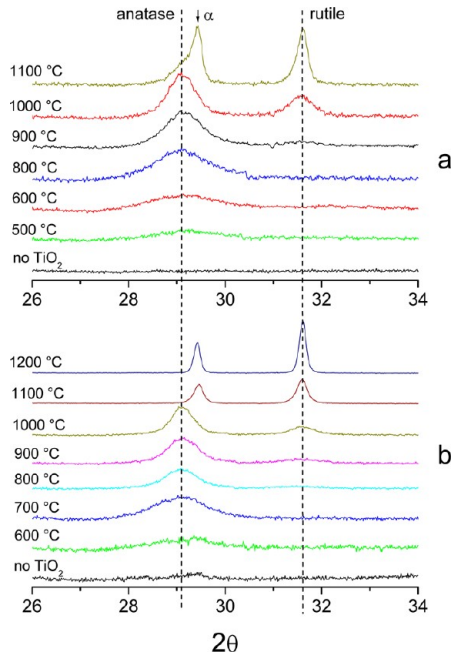

Figure 2. XRD patterns ($\lambda_{CoK\alpha}$ = 1.789 Å) in the range of the main anatase and rutile peaks of nanocomposites A TiO_2–UPA(γ)-SiO_2 (a) and B TiO_2–UPA(θ) (b) after treatment at different temperatures from 400 to 1200 °C.

The anatase-to-rutile phase transformation in powder-like aggregated titania samples is a known kinetics-controlled process, which becomes significant at temperatures ~600 °C but can be observed with a low efficiency at T = 465 °C.[20] On the other hand, anatase becomes more stable than rutile in free titania particles of size below about 14 nm.[21] Our recently reported results on TiO_2 nanoparticles impregnated in silica-treated θ-alumina (sample C) confirm this conclusion: the phase stability is found inverted, and rutile appears when particle size increases to ~17 nm because of agglomeration, which becomes significant at temperatures above 1000 °C.[25]

The situation is found different in θ-alumina without silica treatment (sample B). In this case, first signs of rutile titania were observed at a lower temperature of ~800 °C (Figure 2b). At the same time, a strong increase of the rutile signal begins at a higher temperature, similar to that observed in silica treated θ alumina (sample C). We relate this behavior to the phase transformation acceleration by contact with alumina support. According to our observations, alumina facilitates titania anatase-to-rutile phase transition, and vice versa, titania rutile accelerates alumina densification into the α polymorph. This effect is similar to the alumina sintering acceleration in presence of TiO_2.[36,37] Moreover, the acceleration effect of the most dense alumina α polymorph on the titania apparent phase transition in stronger. We believe that in this particular case the anatase-to-rutile transformation first nucleates on inclusions of α polymorph into γ-alumina. Indeed, traces of α alumina manifest themselves by a weak XRD peak at 2θ = 29.4° in Figure 2b. The TiO_2 nanoparticles spontaneously deposited on these grains transform into rutile polymorph at lower temperatures compared to the majority of the nanoparticles deposited on θ grains. The last are transformed at high temperatures above 1000 °C. This bimodal particle distribution is responsible for the mixed macroscopic anatase/rutile response from sample B. The fact that both anatase and rutile crystallites size are similar supports the conclusion about independent particles aggregation and phase transformation processes. We remark that the strong alumina α polymorph crystallization in sample B begins at the same temperature as the TiO_2 anatase-to-rutile transformation (T ~ 1100 °C), whereas pure alumina samples maintain the θ phase until 1150 °C. Therefore, we conclude our discussion about the mutual promotion of α alumina and rutile TiO_2 polymorphs.

In silica treated γ-alumina (sample A) the rutile polymorph appears at T = 900 °C (Figure 2a), which is higher compared to sample B and lower than that of sample C. The anatase particle size at the phase transition is 9 nm, which is lower than the critical one of 14 nm. It was concluded therefore that the corresponding phase transition is mediated by the contact with the alumina support, similar to sample B. The mutual phase transition acceleration effect between alumina and titania is seen in both appearances of TiO_2 rutile at 900 °C and alumina α at 1100 °C; at the same time, this effect of sample A is weaker (see Figure 2).

The difference between silica treated samples A and C lies in a different thickness of the surface silica layer. Indeed, the TEMS treatment of raw amorphous alumina results in the monolayer coverage of the alumina surface specific area ~300 m^2/g. At subsequent calcinations, the specific area of the alumina decreases (Table 1): ~2 (1150 °C) and ~3 times (1300 °C). This explains the thicker separation layer of silica in sample C compared to sample A. Apparently, at least three molecular layers of silica are required to safely separate the matrix and the supported nanoparticules to preserve the phase stability of titania anatase and mechanical stability of the matrix.

The confirmation of the lowest temperature (compared to three other UPA samples) of the rutile phase appearance in TiO_2 nanoparticles deposited on α-alumina is found in sample D, where the rutile peak at 31.6° was observed at $T \geq$ 800 °C (the corresponding XRD patterns are not shown). Moreover, the rutile content in the sample did not changed, as shown by the intensity comparison of the main rutile TiO_2 and α alumina peaks. At the same time, the anatase TiO_2 peak is screened by the strong peak of α alumina at 29.4°, which prevents the rutile

dx.doi.org/10.1021/cs300033y | ACS Catal. 2012, 2, 1884–1892

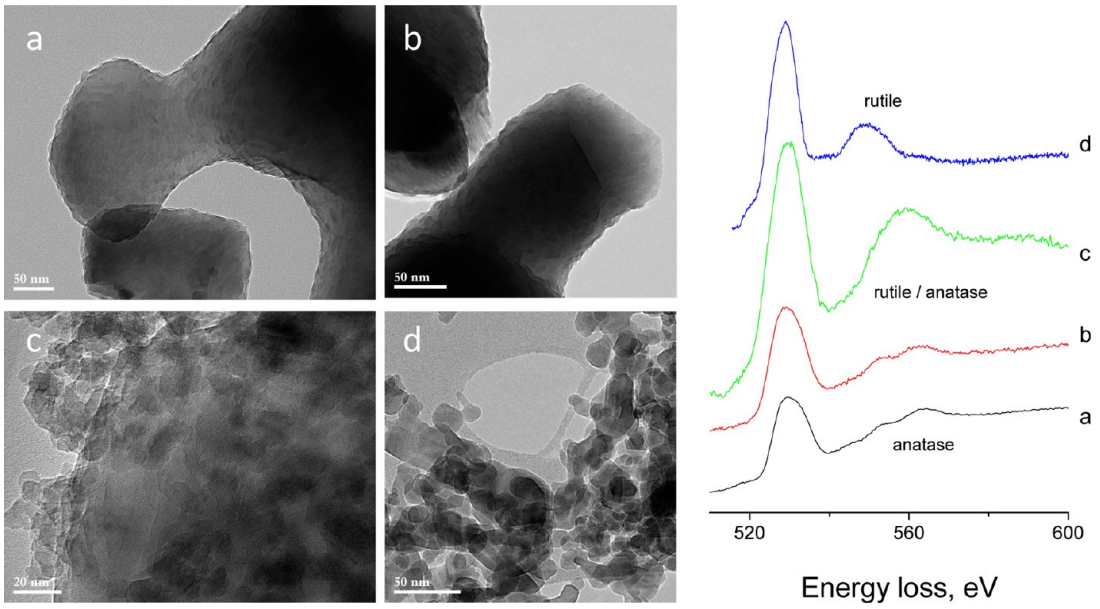

Figure 3. TEM images of nanocomposite TiO_2–UPA(α) after thermal treatment at temperatures 600 °C (a), 700 °C (b,c), and 800 °C (d) and their respective electron energy-loss spectra (right).

ratio analysis at T < 800 °C. In these conditions, the anatase TiO_2 observation in sample D was realized by TEM and EELS spectra measurements[38] shown in Figure 3. The TEM images show evidence of Al_2O_3 matrix uniformly covered by well dispersed 5-nm particles at 600 °C (Figure 3a). At 700 °C two populations of dispersed 5 nm (Figure 3b) and aggregated 10–20 nm (Figure 3c) TiO_2 particles were observed. At 800 °C and higher temperatures, only aggregated larger 20 nm TiO_2 nanoparticles can be seen (Figure 3d). The EELS spectra taken from these images a–d are shown in the right part of Figure 3. They show evidence of typical anatase structure corresponding to images a and b and rutile structure corresponding to images c and d.[38] We therefore conclude that the anatase-to-rutile phase transformation begins at temperatures higher than ~600 °C and completes at 800 °C.

3.2. Photocatalytic Activity. The normalized photocatalytic activity r_S defined by eq 2 of the prepared samples A, B, C, and D is shown as a function of calcination temperature in Figures 4–7. The TiO_2 anatase and rutile crystalline domain size as well as rutile ratio are also plotted in these figures. The maximum activity of the catalysts A, B, and C is shifted to high temperatures of 600–900 °C. This abnormal behavior contrasts to that of sample D, which exhibits characteristic behavior of powder-like samples.

As it is known, the optimal catalyst treatment temperature is explained by a competition between an improvement of the sample crystallinity and decrease of the catalyst surface area due to the grain growth. Because of the weak nanoparticles' aggregation, our nanoparticulate catalysts better conserve the active area at higher temperatures while the crystallinity improves. This may explain the extension of the range and the shift of the maximum activity to higher temperatures of 600, 800, and 900 °C respectively for photocatalysts C, B, and A. The lower optimal temperature of 500 °C is found in most aggregated sample D.

An important issue concerns the optimal polymorphism of the photocatalyst particles, which by analogy with P25 Degussa is largely suggested to be a combination of anatase and rutile phases. Much research has been done to find out the best

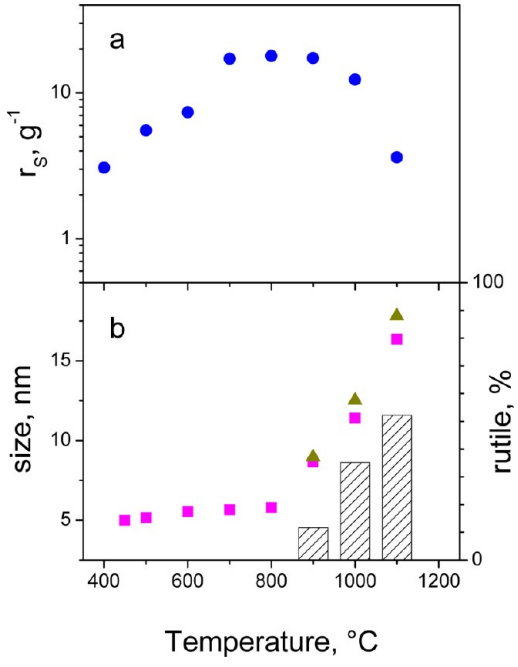

Figure 4. Specific reactivity (a) and anatase (■) and rutile (▲) particle size (b) of nanocomposite TiO_2–UPA(γ)-SiO_2 photocatalyst versus treatment temperature.

percentage of the two phases.[8,11,38] Our present results clearly confirm the thesis about maximum activity of the pure anatase phase of nanoparticulate titania. Indeed, a strong decrease of the photocatalytic activity has been observed in samples A and C at 1100 °C and in sample D at 600 °C. This corresponds to the first appearance of the rutile phase in these samples. The case of the sample B seems to be different, while its best activity corresponds to ~15 wt % of rutile. However, the particle's composition of this sample is heterogeneous according to our XRD analysis: the crystallites in contact with γ alumina conserve anatase structure while those deposited onto α alumina impurities become rutile. The equal size of the anatase

dx.doi.org/10.1021/cs300033y | ACS Catal. 2012, 2, 1884–1892

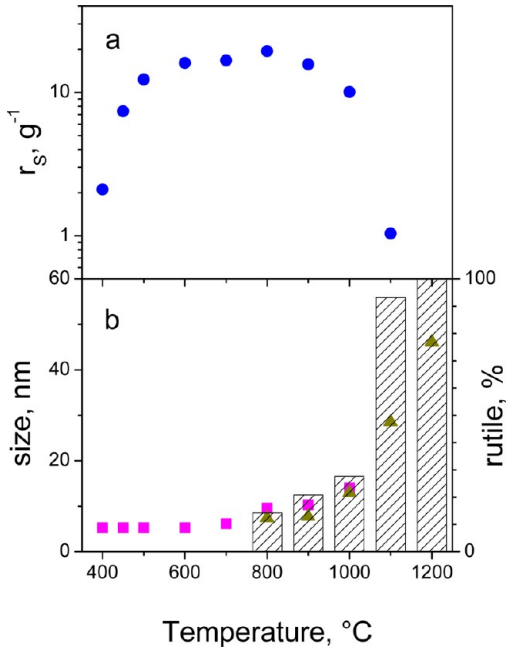

Figure 5. Specific reactivity (a) and anatase (■) and rutile (▲) particle size (b) of nanocomposite TiO_2–UPA(θ) photocatalyst versus treatment temperature.

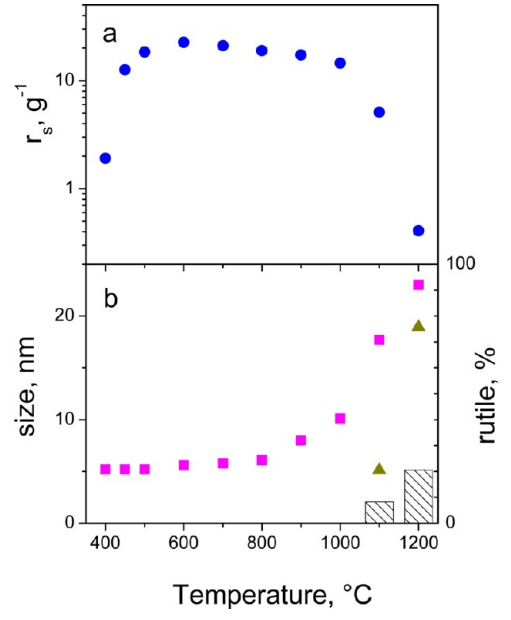

Figure 6. Specific reactivity (a) and anatase (■) and rutile (▲) particle size (b) of nanocomposite TiO_2–UPA(θ)-SiO_2 photocatalyst versus treatment temperature.

and rutile crystallites to that of the amorphous colloidal nanoparticles confirms the key role of catalyst-substrate interaction in the nanoparticle phase stability.

In contrast, the samples A, B, C, and D consist of pure anatase or rutile polymorphs, with the exception of catalyst C treated at 1100 °C. In this case, the rutile phase appears at 1100 °C when the anatase nanoparticle size becomes 17 nm. The silica treatment apparently avoids direct contact between titania and alumina, which prohibits the accelerative interaction between α-alumina and rutile TiO_2 polymorphs, discussed above. In these conditions, the rutile phase nucleates onto the

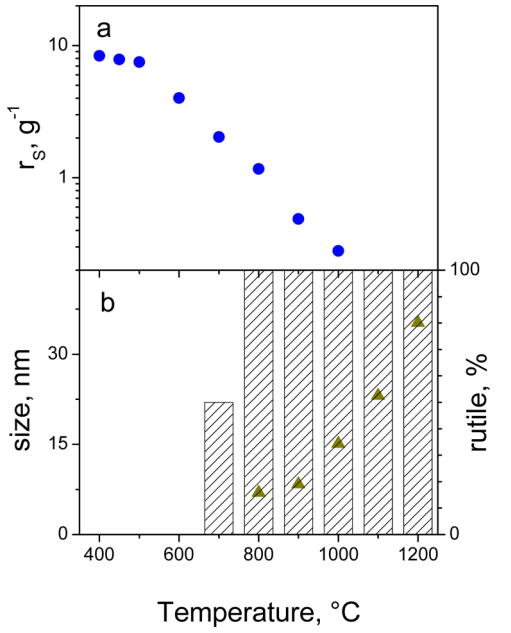

Figure 7. Specific reactivity (a) and rutile particle size (b) of nanocomposite TiO_2–UPA(α) photocatalyst versus treatment temperature.

anatase one. This is confirmed by the smaller size of the rutile domains (5 nm) compared to the anatase one (17 nm). We believe that the rutile nucleation begins at the grains boundaries as suggested by Zhang et al.[23] The initial size of the rutile domain corresponds to the size of primary nanoparticles, which may signify that the adjacent nanoparticle is entirely transformed. Clearly, the nucleation of rutile phase onto anatase titania nanoparticles produces a negative effect of their photocatalytic activity.

A better insight into the size and polymorphism effect on the titania photocatalytic activity can be seen in Figure 8, where the normalized photocatalytic activity r_S is summarized as a function of the crystalline size for all prepared samples A, B, C, and D. The experimental data fit two branches of high and low photocatalytic activity. In particular, the experimental series of sample D entirely follows branch 2 and experimental series of samples A, B, and C ($T \leq 1000$ °C) constitute branch 1. The

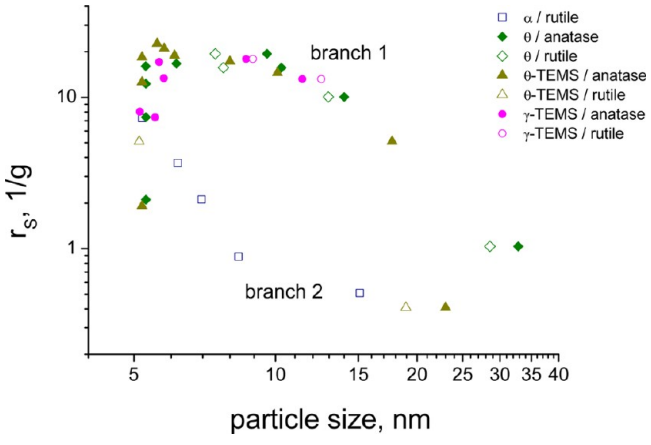

Figure 8. Specific reactivity of TiO_2 particles of different sizes of anatase and rutile polymorphs deposited on UPA supports of γ, θ, and α polymorphs, treated or non with TEMS.

dx.doi.org/10.1021/cs300033y | ACS Catal. 2012, 2, 1884–1892

experimental points of samples A, B, and C (T > 1000 °C) fit either branches 1 or 2 or both. The last is the case of sample C containing anatase and rutile, which sizes are respectively of 17 and 5 nm.

Several features can be highlighted:

- Activities of anatase and rutile phases approach for the smallest nanoparticles about 5 nm.
- Activity of anatase titania (branch 1) almost does not depend on size until 10 nm.
- Activity of rutile titania (branch 2) decreases with size above 5 nm.
- Difference between the anatase and rutile activities increases with size.
- Activity of the mixed polymorph particles follows the same branches, in agreement with the respective sizes of anatase and rutile domains.

We add that the apparent strong decrease of the anatase activity of size above 10 nm is not inherent to this crystalline phase but is due to the rutile phase nucleation.

An important conclusion can be drawn: (1) activity of mixed populations of anatase and rutile nanoparticles depends on the anatase size; and (2) activity of the composite nanoparticles containing anatase and rutile polymorphs depends on the rutile crystalline size. The first conclusion is explained by the fact that most active anatase nanoparticles mask the response of less active rutile nanoparticles. The second conclusion may be explained by the dominant charge and excitation transfer to the less active polymorph. In complement to the liquid-phase photocatalysis,[8] the present work shows that the pure anatase activity in gas-phase photocatalysis is superior to that of rutile TiO_2 and composite rutile/anatase nanoparticles.

The decrease of the photocatalytic activity of anatase TiO_2 nanoparticles with increase of the size has been tentatively explained in the framework of the electron localization model.[16,25] The smaller electron localization radius in rutile compared with that of anatase crystallites[39] may support the observed faster activity decrease with size of the rutile nanoparticles compared with that of anatase ones (Figure 8). On the other hand, the decrease of the specific photocatalyst area cannot be responsible for the observed reduction of the photocatalytic activity, in agreement with ref 25.

3.3. Comparison with Degussa P25 TiO_2. A comparison can be made between the photocatalytic efficiencies of best prepared samples and the reference industrial catalyst Degussa P25 TiO_2. The direct comparison of the specific reactivities according to eq 2 is not realistic since the photocatalysts morphologies are different. In particular, the homogeneous impregnation of P25 Degussa nanoparticles into the UPA matrixes is not possible: this product is agglomerated and it does not form strong bonds with the support. Therefore, we have prepared the coated glass beads (D = 1 mm) by P25 Degussa. The preparation is realized in the aqueous slurry containing 5% Degussa P25 TiO_2, preliminarily washed with 5 M H_2SO_4 at 50 °C; the coated beads were then fired at 450 °C for 4 h. The mass of the deposited catalyst was ~7.0 μg/sphere. The mean thickness of nanocoatings of ~2 μm has been calculated by taking into account the TiO_2 mass density of 3.9 g/cm^3. The reactor yield attains 95% of continuous performance in the experimental conditions similar to those of the TiO_2–UPA catalyst test.

As Benmami et al.[34] have pointed out, the comparison of internal material efficiencies Γ requires knowledge of the material absorption efficiency A ($R \propto A{\cdot}\Gamma$), which can be estimated from

$$A = \frac{k_{abs}}{k_{abs} + k_{scatt}} \quad (3)$$

where k_{abs} and k_{scatt} are respectively light absorption and scattering coefficients. Then, relative material efficiencies can be obtained by normalizing the reactivity R from eq 1 on A from eq 3.

An example of the absorbance spectra of the silica-treated θ-alumina matrix (a) and TiO_2–UPA sample C treated at 500 °C (b) is shown in Figure 9. Similar spectra were obtained for our

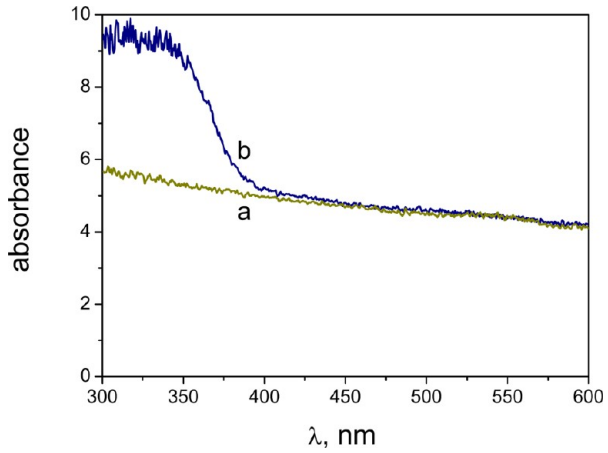

Figure 9. Absorption spectra of UPA(θ)–SiO_2 matrix (a) and TiO_2–UPA(θ)-SiO_2 photocatalyst thermally treated at 500 °C (b).

γ-alumina. The pure alumina matrix is found strongly scattering and low absorbing medium. The corresponding extinction curve a in Figure 9 follows the common normal dispersion relation ($dn/d\lambda < 0$). A remarkable modification of the matrix transparency in the UVA spectral range at $\lambda \leq 380$ nm (curve b in Figure 9) at the nanoparticles' impregnation is characteristic of the anatase interband absorption. Accordingly, the measured absorption efficiencies (3) of the TiO_2–UPA and P25 catalysts at the photocatalytic lamp wavelength (362 nm) are respectively A_{TiO_2-UPA} = 0.32 ($k_{abs} < k_{scatt}$) and A_{P25} = 0.9 ($k_{abs} \gg k_{scatt}$).

The best samples C (and A) with the TiO_2 mass loading ~25 wt % thermally treated between 500 and 1000 °C show the reactivity R_{TiO_2-UPA} = 2.2 whereas the reactivity of the P25 Degussa TiO_2 sample in the same photocatalytic experiment conditions is somewhat higher, R_{P25} = 3.0 (this corresponds to the measured ethylene decomposition yield 95%). This sets the ratio of the materials photocatalytic efficiencies to $\Gamma_{TiO_2-UPA}/\Gamma_{P25}$ = 2. The enhanced efficiency of the nanoparticulate TiO_2–UPA photocatalysts is explained by its nonagglomerated morphology. Low light absorption by nanoparticles can be readily compensated by an increased lifetime of the lamp photons in the material in the strongly scattered radiation transport regime ($k_{abs} \ll k_{scatt}$).

The excellent activity of P25 Degussa compared to the composite anatase/rutile nanoparticles prepared in this work may be related to the amorphous component, whose existence is often neglected. In contrast to P25 Degussa, this component is expected to vanish in our samples treated above 1000 °C, where the rutile nucleation begins. This amorphous titania

dx.doi.org/10.1021/cs300033y | ACS Catal. 2012, 2, 1884–1892

serves to be an excellent attractor for photoinduced electrons,[40] which conserve their chemical activity.

Titania-alumina composites have been previously considered for catalytic applications.[41−44] Most recently, Smitha et al.[45] have reported an enhanced photocatalytic activity of hydrophobic titania−alumina coatings with 5−30 mol % alumina, which preserve 100% anatase TiO_2 at 800 °C. These results are in agreement with our previously published data.[25] The present study sheds more light on nanoscale morphology of titania-alumina materials in correlation with photocatalytic activity.

4. CONCLUSION

The low density and high porosity, small size of the structural unit and evanescent intrinsic absorption in the UVA spectral range make monolithic alumina interesting for applications as supporting materials for photocatalyst nanoparticles.

In the present work, new nanoparticulate photocatalytic media were prepared by impregnation of size-selected TiO_2 nanoparticles with a mass of ∼25 wt % into monolithic ultraporous alumina (UPA). We observed the effect of the nanoparticles' polymorphism and size on this activity. Use of UPA supports of γ, θ, and α polymorphs, covered with silica or not, and thermal treatment at different temperatures allow modification of the nanonparticles' size and crystalline composition. The electronic coupling between titania and UPA support is found to affect the nanoparticle polymorph. In particular, a separation layer of silica increases the TiO_2 anatase stability.

The main conclusion is that pure anatase nanoparticles exhibit the higher activity compared with that of rutile and composite anatase/rutile nanoparticles. In particular, the photocatalytic activity strongly decreases as soon as the rutile phase is nucleated onto anatase. The activity of the mixed populations of anatase and rutile nanoparticles depends on the anatase size, while the activity of the composite nanoparticles containing anatase and rutile polymorphs depends on the rutile crystalline size. In pure rutile nanoparticles the activity strongly decreases with size $2R \geq 5$ nm, while in pure anatase it remains constant for sizes $2R \leq 10$ nm. A comparative study shows significantly higher photocatalytic efficiency of the prepared materials compared to that of the reference P25 Degussa photocatalyst.

AUTHOR INFORMATION

Corresponding Author

*E-mail: andrei.kanaev@lspm.cnrs.fr.

Funding

This work is supported by the COST D41 Action of the European Commission and C'Nano network (IdF, France). M.B. thanks IPEIN of the University El Manar of Tunis for financial support of his Ph.D. work. The authors acknowledge the financial support of the IFR Paris-Nord Plaine de France.

Notes

The authors declare no competing financial interest.

REFERENCES

(1) Fujishima, A.; Hashimoto, K.; Watanabe, T. *TiO_2 Photocatalysis: Fundamentals and Applications*; BKC: Tokyo, 1999.
(2) Fujishima, A.; Rao, T. N.; Tryk, D. A. *J. Photochem. Photobiol., C* **2000**, *1*, 1.
(3) Henderson, M. A. *Surf. Sci. Rep.* **2011**, *66*, 185.
(4) Bickley, R. I.; Gonzalez-Carreno, T.; Lees, J. S.; Palmisano, L.; Tilley, R. J. D. *J. Solid State Chem.* **1991**, *92*, 178.
(5) Ohtani, B.; Prieto-Mahaney, O. O.; Li, D.; Abe, R. *J. Photochem. Photobiol., A* **2010**, *216*, 179.
(6) Ohtani, B.; Ogawa, Y.; Nishimoto, S.-I. *J. Phys. Chem. B* **1997**, *101*, 3746.
(7) Hurum, D. C.; Agrios, A. G.; Gray, K. A.; Rajh, T.; Thurnauer, M. C. *J. Phys. Chem. B* **2003**, *107*, 4545.
(8) Carneiro, J. T.; Savenije, T. J.; Moulijn, J. A.; Mul, G. *J. Phys. Chem. C* **2011**, *115*, 2211.
(9) Tanaka, K.; Capule, M. F. V.; Hisanaga, T. *Chem. Phys. Lett.* **1991**, *187*, 73.
(10) Piscopo, A.; Robert, D.; Weber, J. V. *J. Photochem. Photobiol., A* **2001**, *139*, 253.
(11) Jang, H. D.; Kim, S.-K.; Kim, S.-J. *J. Nanopart. Res.* **2001**, *3*, 141.
(12) Zhu, Q.; Qian, J.; Pan, H.; Tu, L.; Zhou, X. *Nanotechnology* **2011**, *22*, 395703.
(13) Zhang, Z.; Wang, C.-C.; Zakaria, R.; Ying, J. Y. *J. Phys. Chem. B* **1998**, *102*, 10871.
(14) Liu, G.; Sun, C.; Yang, H. G.; Smith, S. C.; Wang, L.; Lu, G. Q. (Max); Cheng, H.-M. *Chem. Commun.* **2010**, *46*, 755.
(15) Marugan, J.; Hufschmidt, D.; Sagawe, G.; Selzer, V.; Bahnemann, D. *Water. Res.* **2006**, *40*, 833.
(16) Tieng, S.; Kanaev, A.; Chhor, K. *Appl. Catal. A* **2011**, *399*, 191.
(17) Carneiro, J. T.; Savenije, T. J.; Moulijn, J. A.; Mul, G. *J. Phys. Chem. C* **2010**, *114*, 327.
(18) Monticone, S.; Tufeu, R.; Kanaev, A. V.; Scolan, E.; Sanchez, C. *Appl. Surf. Sci.* **2000**, *162−163*, 565.
(19) Satoh, N.; Nakashima, T.; Kamikura, K.; Yamamoto, K. *Nat. Nanotechnol.* **2008**, *3*, 106.
(20) Gribb, A. A.; Banfield, J. F. *Am. Mineral.* **1997**, *82*, 717.
(21) Zhang, H.; Banfield, J. F. *J. Mater. Chem.* **1998**, *8*, 2073.
(22) Zhang, J.; Xu, Q.; Li, M.; Feng, Z.; Li, C. *J. Phys. Chem. C* **2009**, *113*, 1698.
(23) Zhang, J.; Li, M.; Feng, Z.; Chen, J.; Li, C. *J. Phys. Chem. B* **2006**, *110*, 927.
(24) Lopez-Munoz, M.-J.; van Grieken, R.; Aguado, J.; Marugen, J. *Catal. Today* **2005**, *101*, 307.
(25) Bouslama, M.; Amamra, R.; Tieng, S.; Brinza, O.; Chhor, K.; Abderrabba, M.; Vignes, J.-L.; Kanaev, A. *Appl. Catal., A* **2011**, *402*, 156.
(26) Vignes, J.-L.; Frappart, C.; di Costanzo, T.; Rouchaud, J.-C.; Mazerolles, L.; Michel, D. *J. Mater. Sci.* **2008**, *43*, 1234.
(27) di Costanzo, T.; Fomkin, A. A.; Frappart, C.; Khodan, A. N.; Kuznetsov, D. G.; Mazerolles, L.; Michel, D.; Minaev, A. A.; Sinitsin, V. A.; Vignes, J.-L. *Mater. Sci. Forum* **2004**, *453−454*, 315.
(28) Rivallin, M.; Benmami, M.; Kanaev, A.; Gaunand, A. *Chem. Eng. Res. Des.* **2005**, *83*, 67.
(29) Azouani, R.; Michau, A.; Hassouni, K.; Chhor, K.; Bocquet, J.-F.; Vignes, J.-L.; Kanaev, A. *Chem. Eng. Res. Des.* **2010**, *88*, 1123.
(30) Azouani, R.; Soloviev, A.; Benmami, M.; Chhor, K.; Bocquet, J.-F.; Kanaev, A. *J. Phys. Chem. C* **2007**, *111*, 16243.
(31) Pucher, P.; Benmami, M.; Azoauni, R.; Krammer, G.; Chhor, K.; Bocquet, J.-F.; Kanaev, A. V. *Appl. Catal., A* **2007**, *332*, 297.
(32) Coronado, J. M.; Zorn, J. M.; Tejedor-Tejedor, I.; Anderson, M. *Appl. Catal., B* **2003**, *43*, 329.
(33) Benmami, M.; Chhor, K.; Kanaev, A. *AIDIC Conf. Series: Selected Papers of IcheaP7* **2005**, *7*, 29.
(34) Benmami, M.; Chhor, K.; Kanaev, A. V. *Chem. Phys. Lett.* **2006**, *422*, 552.
(35) Spurr, R. A.; Myers, H. *Anal. Chem.* **1957**, *29*, 760.
(36) Horn, D. S.; Messing, G. L. *Mater. Sci. Eng., A* **1995**, *195*, 169.
(37) Mann, M.; Shter, G. E.; Grader, G. S. *J. Mater. Sci.* **2002**, *37*, 4049.
(38) Kawahara, T.; Ozawa, T.; Iwasaki, M.; Tada, H.; Ito, S. *J. Colloid Interface Sci.* **2003**, *267*, 377.
(39) Tang, H.; Prasad, K.; Sanjinès, R.; Schmid, P. E.; Lévy, F. *J. Appl. Phys.* **1994**, *75*, 2042.
(40) Kuznetsov, A.; Kameneva, O.; Alexandrov, A.; Bityurin, N.; Chhor, C.; Kanaev, A. *J. Phys. Chem. B* **2006**, *110*, 435.

(41) Choi, J.; Kim, J.; Yoo, K. S.; Lee, T. G. *Powder Technol.* **2008**, *181*, 83.
(42) Hu, H.; Xiao, W.; Yuan, J.; Shi, J.; He, D.; Shangguan, W. *J. Sol-Gel. Sci. Technol.* **2008**, *45*, 1.
(43) Choi, H.; Stathatos, E.; Dionysiou, D. *Appl. Catal., B* **2006**, *63*, 60.
(44) Tursiloadi, S.; Imai, H.; Hirashima, H. *J. Non-Cryst. Solids* **2004**, *350*, 271.
(45) Smitha, V. S.; Baiju, K. V.; Perumal, P.; Ghosh, S.; Warrier, K. G. *Eur. J. Inorg. Chem.* **2012**, *2012*, 226.